

₁ Study of neutrino-nucleus interaction at around 1 GeV using
₂ a 3D grid-structure neutrino detector, WAGASCI, muon
₃ range detectors and magnetized spectrometer, Baby MIND,
₄ at J-PARC neutrino monitor hall

₅ A. Bonnemaison, R. Cornat, L. Domine, O. Drapier, O. Ferreira, F. Gastaldi,
₆ M. Gonin, J. Imber, M. Licciardi, F. Magniette, T. Mueller, L. Vignoli, and O. Volcy
₇ *Ecole Polytechnique, IN2P3-CNRS, Laboratoire Leprince-Ringuet, Palaiseau,*
₈ *France*

₉ S. Cao and T. Kobayashi

₁₀ *High Energy Accelerator Research Organization (KEK), Tsukuba, Ibaraki, Japan*

₁₁ M. Khabibullin, A. Khotjantsev, A. Kostin, Y. Kudenko, A. Mefodiev, O. Mineev,
₁₂ S. Suvorov, and N. Yershov

₁₃ *Institute for Nuclear Research of the Russian Academy of Sciences, Moscow, Russia*

₁₄ B. Quilain

₁₅ *Kavli Institute for the Physics and Mathematics of the Universe (WPI), The*
₁₆ *University of Tokyo Institutes for Advanced Study, University of Tokyo, Kashiwa,*
₁₇ *Chiba, Japan*

₁₈ T. Hayashino, A. Hiramoto, A.K. Ichikawa, K. Nakamura, T. Nakaya, K Yasutome,
₁₉ and K. Yoshida

₂₀ *Kyoto University, Department of Physics, Kyoto, Japan*

₂₁ Y. Azuma, J. Harada, T. Inoue, K. Kin, N. Kukita, S. Tanaka, Y. Seiya,
₂₂ K. Wakamatsu, and K. Yamamoto

₂₃ *Osaka City University, Department of Physics, Osaka, Japan*

24 A. Blondel, F. Cadoux, Y. Favere, E. Noah, L. Nicola, and S. Parsa

25 *University of Geneva, Section de Physique, DPNC, Geneva, Switzerland*

26 N. Chikuma, F. Hosomi, T. Koga, R. Tamura, and M. Yokoyama

27 *University of Tokyo, Department of Physics, Tokyo, Japan*

28 Y. Hayato

29 *University of Tokyo, Institute for Cosmic Ray Research, Kamioka Observatory,*
30 *Kamioka, Japan*

31 Y. Asada, K. Matsushita, A. Minamino, K. Okamoto, and D. Yamaguchi

32 *Yokohama National University, Faculty of Engineering, Yokohama, Japan*

33 December 14, 2017

34 **Contents**

35	1	Introduction	3
36	2	Experimental Setup	4
37	2.1	Wagasci modules	5
38	2.1.1	Detector	5
39	2.1.2	Electronics	8
40	2.1.3	Water system	9
41	2.2	INGRID Proton module	10
42	2.3	Baby MIND	11
43	2.3.1	Magnet modules	11
44	2.3.2	Scintillator modules	12
45	2.3.3	Electronics	14
46	2.3.4	Pefromance check	15
47	2.4	Side muon range detector	16

48	3 Physics goals	18
49	3.1 Expected number of events	19
50	3.2 Pseudo-monochromatic beam by using different off-axis fluxes	19
51	3.3 Subjects Wagasci can contribute	20
52	4 Status of J-PARC T59 experiment	22
53	5 MC studies	24
54	5.1 Simulation setup	24
55	5.2 Event selection	28
56	5.3 Cross section measurements	29
57	6 Standalone WAGASCI-module performances	30
58	6.1 Reconstruction algorithm	32
59	6.1.1 Description	32
60	6.1.2 Performances	33
61	6.2 Background subtraction: the water-out module	38
62	7 Schedule	41
63	8 Requests	41
64	8.1 Neutrino beam	41
65	8.2 Equipment request including power line	41

66 **1 Introduction**

67 The understanding of neutrino-nucleus interactions in the 1 GeV energy region is critical
 68 for the success of accelerator-based neutrino oscillation experiments such as the T2K exper-
 69 iment. Complicated multi-body effects of nuclei render this understanding difficult. The
 70 T2K near detectors have been measuring these and significant progress has been achieved.
 71 However, the understanding is still limited. One of the big factors preventing from full
 72 understanding is the non-monochromatic neutrino beam spectrum. Measurements with
 73 different but some overlapping beam spectra would greatly benefit to resolve the contri-
 74 bution from different neutrino energies. We, the Wagasci collaboration, proposes to study
 75 the neutrino-nucleus interaction at the B2 floor of the neutrino monitor building, where
 76 different neutrino spectra can be obtained due to the different off-axis position. Our exper-
 77 imental setup contains 3D grid-structure plastic-scintillator detectors filled with water as
 78 the neutrino interaction target (Wagasci modules), two side- and one downstream- muon
 79 range detectors(MRD's). The 3D grid-structure and side-MRD's allows a measurement of
 80 wider-angle scattering than the T2K off-axis near detector (ND280). High water to scintil-
 81 lator material ratio enables the measurement of the neutrino interaction on water, which

is highly desired for the T2K experiment because it's far detector, Super-Kamiokande, is composed of water. The MRD's consist of plastic scintillators and iron plates. The downstream-MRD, so called the Baby MIND detector, also works as a magnet and provides the charge identification capability as well as magnetic momentum measurement for high energy muons. The charge identification is essentially important to select antineutrino events in the antineutrino beam because contamination of the neutrino events is as high as 30%. Most of the detectors has been already constructed. The Wagasci modules have been commissioned as the J-PARC T59 experiment and the Baby MIND detector was commissioned at the CERN neutrino platform. Therefore, the collaboration will be ready to proceed to the physics data taking for the T2K beam time in January 2019. We will provide the cross sections of the charged current neutrino and antineutrino interactions on water with slightly higher neutrino energy than T2K ND280 with wide angler acceptance. When combined with ND280 measurements, our measurement would greatly improve the understanding of the neutrino interaction at around 1 GeV and contribute to reduce one of the most significant uncertainty of the T2K experiment.

2 Experimental Setup

Figure. 1 and 2 show a schematic view and a CAD drawing of the entire set of detectors. Central neutrino target detectors consist of two Wagasci modules and T2K INGRID proton module. Inside the Wagasci module, plastic scintillator bars are aligned as a 3D grid-like structure and spaces in the structure are filled with water for a water-in Wagasci module. T2K INGRID proton module is a full active neutrino target detector which is composed only with scintillator bars in its tracking region. The central detectors are surrounded by two side- and one downstream- muon range detectors(MRD's) The MRD's are used to select muon tracks from the charged-current (CC) interactions and to reject short tracks caused by neutral particles that originate mainly from neutrino interactions in material surrounding the central detector, like the walls of the detector hall, neutrons and gammas, or neutral-current (NC) interactions. The muon momentum can be reconstructed from its range inside the detector. The MRD's consist of plastic scintillators and iron plates. In addition, each of the iron plates of the downstream-MRD, so called the Baby MIND detector, is wound by a coil and can be magnetized. It provide the charge selection capability.

For all detectors, scintillation light in the scintillator bar is collected and transported to a photodetector with a wavelength shifting fiber (WLS fiber). The light is read out by a photodetector, Multi-Pixel Photon Counter (MPPC), attached to one end of the WLS fiber. The signal from the MPPC is read out by the dedicated electronics developed for the test experiment to enable bunch separation in the beam spill. The readout electronics is triggered using the beam-timing signal from MR to synchronize to the beam. The beam-timing signal is branched from those for T2K, and will not cause any effect on the T2K data taking.

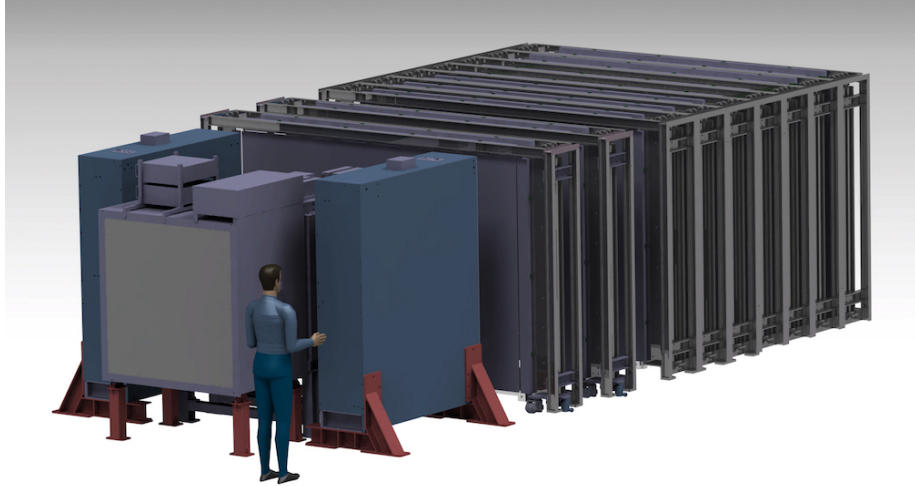


Figure 1: Schematic view of entire sets of detectors.

120 T2K adopted the off-axis beam method, in which the neutrino beam is intentionally
 121 directed 2.5 degrees away from SK producing a narrow band ν_μ beam. The off-axis near
 122 detector, ND280, is installed towards the SK direction in the B1 floor of the near detector
 123 hall of the J-PARC neutrino beam-line. We propose to install our detector in the B2 floor
 124 of the near detector hall, where the off-axis angle is similar but slightly different: 1.5 degree.
 125 The candidate detector position in the B2 floor is shown in Fig. 3. The expected neutrino
 126 energy spectrum at the candidate position is shown in Fig. 4.

127 **2.1 Wagasci modules**

128 **2.1.1 Detector**

129 The WAGASCI modules are mainly composed of 1280 plastic scintillator bars and a sur-
 130 rounding stainless steel tank as shown in Fig. 5. The total number of channels in one
 131 Wagasci module is 1280. The stainless steel tank is constructed by welding stainless steel
 132 plates, is sized as $46 \times 125 \times 125$ cm 3 , and weighs 0.5 ton.

133 One Wagasci module consists of 16 scintillator tracking planes, where each plane is an
 134 array of 80 scintillator bars fixed with ABS frames. The 40 bars, called parallel scintillators,
 135 are placed perpendicularly to the beam, and the other 40 bars, called grid scintillators, are
 136 placed in parallel to the beam with grid structure in the tracking plane as shown in Fig.
 137 5. Thanks to the 3 D grid-like structure of the scintillator bars, the Wagasci module has
 138 4π angular acceptance for charged particles.

139 Thin plastic scintillator bars produced at Fermilab by extrusion method, mainly consists

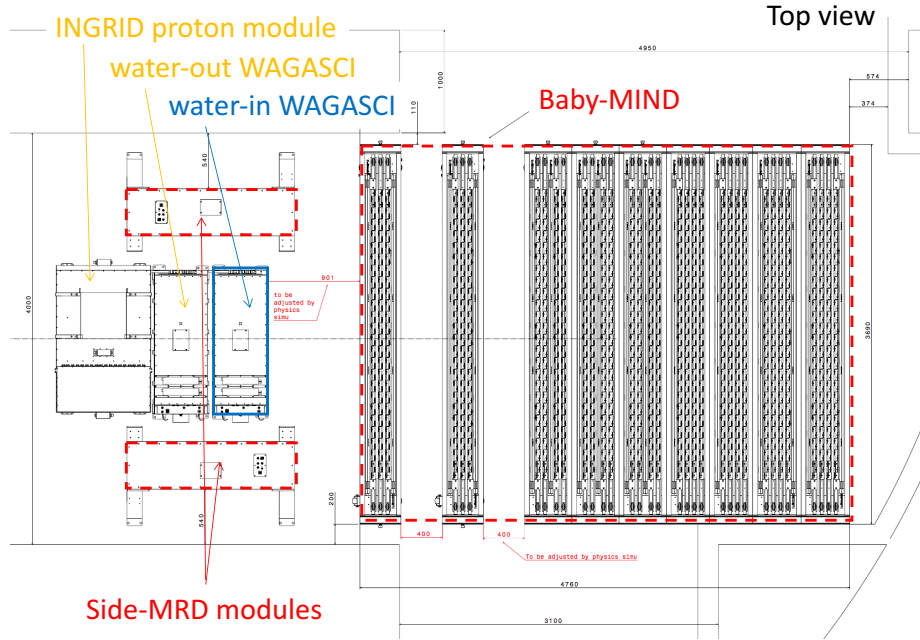


Figure 2: Top view of entire sets of detectors.

of polystyrene and are surrounded by thin reflector including TiO^2 (3 mm in thickness) are used for the Wagasci modules to reduce the mass ratio of scintillator bars to water, because neutrino interactions in the scintillator bars are a background for the cross section measurements on H_2O . Each scintillator bar is sized as $1020 \times 25 \times 3 \text{ mm}^3$ including the reflector part, and half of all the scintillator bars have 5-cm-interval slits to form the grid structure (Figure 6).

We will have two types of the Wagasci modules, a water-in module and a water-out module. The water-in Wagasci module has water in spaces of the grid structure. The total water mass serving as neutrino targets in the fiducial volume of the module is 188 kg, and the mass ratio of scintillator bars to water is 80 %. The water-out Wagasci module doesn't have water inside the detector. The total CH mass serving as neutrino target in the fiducial volume of the module is 47 kg, and the mass fraction of scintillator bars is 100 %.

Scintillation light is collected by wave length shifting fibers, Y-11 (non-S type with a diameter of 1.0 mm produced by Kuraray. A fiber is glued by optical cement in a groove on surface of a scintillator bar. 32 fibers are gathered together by a fiber bundle at edge of the module, and lead scintillation light to a 32-channel arrayed MPPC. Since crosstalk of light yield due to reflection on the inner surface of each cell has been observed, all the scintillator bars are painted black by aqueous color spray. It is confirmed by measurements

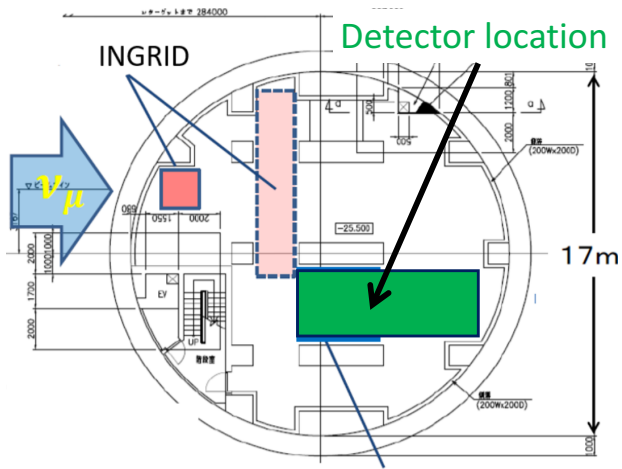


Figure 3: Candidate detector position in the B2 floor of the near detector hall.

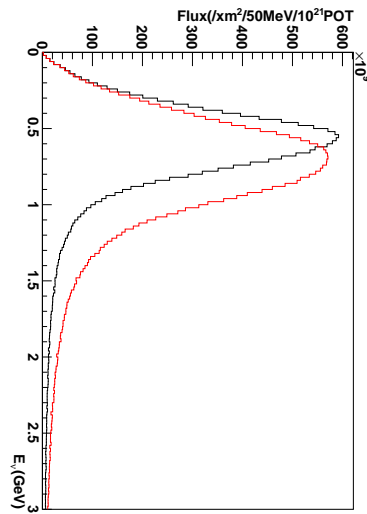


Figure 4: Neutrino energy spectrum at the candidate detector position(red, off-axis 1.5 degree). The spectrum at the ND280 site (black, off-axis 2.5 degree) is also shown.

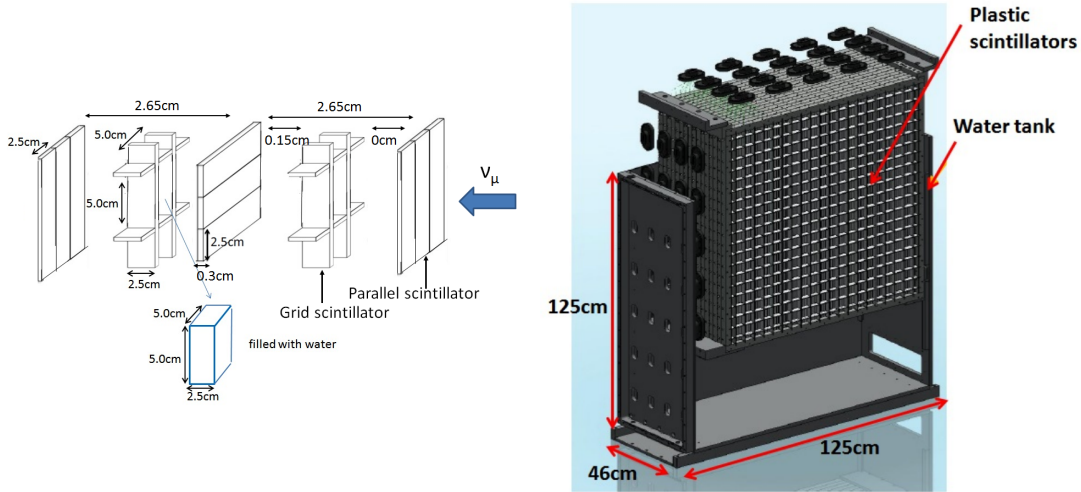


Figure 5: Schematic views of 3D grid-like structure of plastic scintillator bars (left) and Wagasci module (right).

158 with cosmic rays that black painting on the surface of the scintillator bars suppresses this
 159 crosstalk so that no significant crosstalk effect is observed within uncertainty.

160 32-channel arrayed MPPCs, as shown in the Fig. 7, are used for the modules. The
 161 surface of the fiber bundle is polished and directly attached onto the 32-channel arrayed
 162 MPPCs. The positions of 32 fibers on the bundle are aligned to fit the channels of MPPCs.
 163 The MPPC is a product of Hamamatsu Photonics, S13660(ES1), with suppressed noise
 164 rate of ~ 6 kHz per channel at 0.5 p.e. threshold. For each MPPC channel, 716 pixels of
 165 APD are aligned in a shape of circle.

166 2.1.2 Electronics

167 As front-end electronics of this detector, a Silicon PM Integrated Read-Out Chip (SPIROC)
 168 [12] is adopted. SPIROC is a 36-channel auto-triggered front-end ASIC, and is produced
 169 by OMEGA/ IN2P3. It not only contains an analog signal processing part such as amplification
 170 and shaping of the waveform, but contains a digital signal processing parts such as
 171 auto-trigger and timing measurement. Charge of MPPC signal is sampled by track-and-
 172 hold circuit. A Front-end electronics board, Active Sensor Unit (ASU), has been developed
 173 with the SPIROC2D chip, which is the latest version of SPIROC. Each readout board is
 174 designed to control a 32-channel arrayed MPPC, and 40 of the ASU boards are aligned on
 175 the module surface. The data acquisition system used for this detector, including back-end
 176 boards, has been developed for prototypes of ultra-granular calorimeters for the Interna-
 177 tional Linear Collider (ILC) [5], and independent of the T2K DAQ system. To synchronize

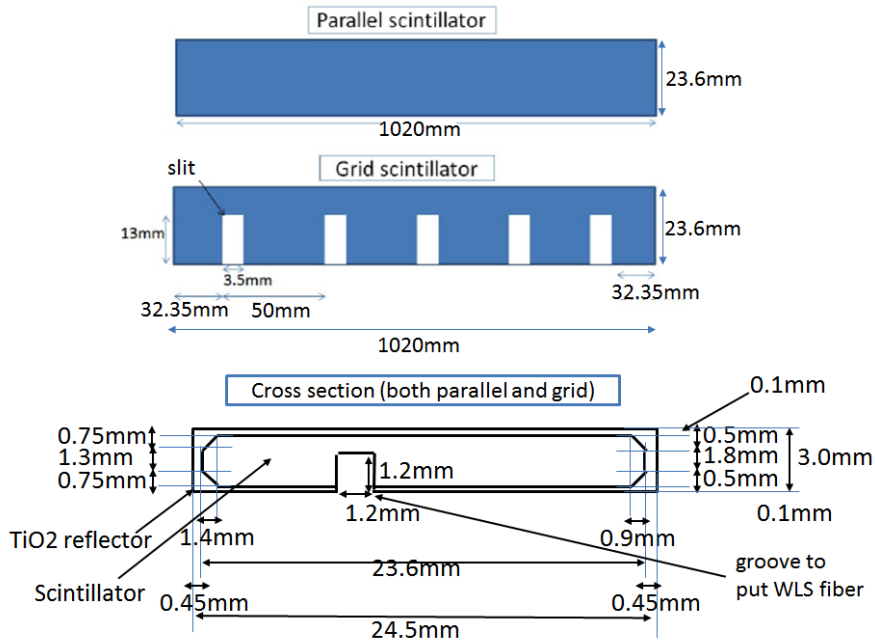


Figure 6: Geometry of scintillators used for Wagasci modules.

178 the DAQ system to J- PARC neutrino beam, pre-beam trigger and beam trigger are sent to
 179 the clock control card. The beam trigger signals are converted from optical signals to NIM
 180 signals at NIM module on the B2 floor. In addition, the information of spill number are
 181 delivered with 16-bit ECL level signals, and converted to an Ethernet frame by an FPGA
 182 evaluation board to be directly sent to the DAQ PC. The electronics readout scheme is
 183 shown in Fig. 8.

184 **2.1.3 Water system**

185 Pure water is filled to the water tank of the water-in Wagasci module as follows. First,
 186 the water storage tank located at the B2 floor of the NM pit is filled with water delivered
 187 from a water tap on the ground level through a long hose. Second, the water is pumped
 188 to the other water storage tank though a water filler to produce pure water. Third, a
 189 compound preservative called Germall plus, which is the same preservative used in one of
 190 the sub-detectors of T2K ND280, FGD2, is put into the water to keep water from being
 191 bad. Then, the water is poured to the water-in Wagasci module, and it is kept in the
 192 module during the neutrino beam operation and not to be circulated.

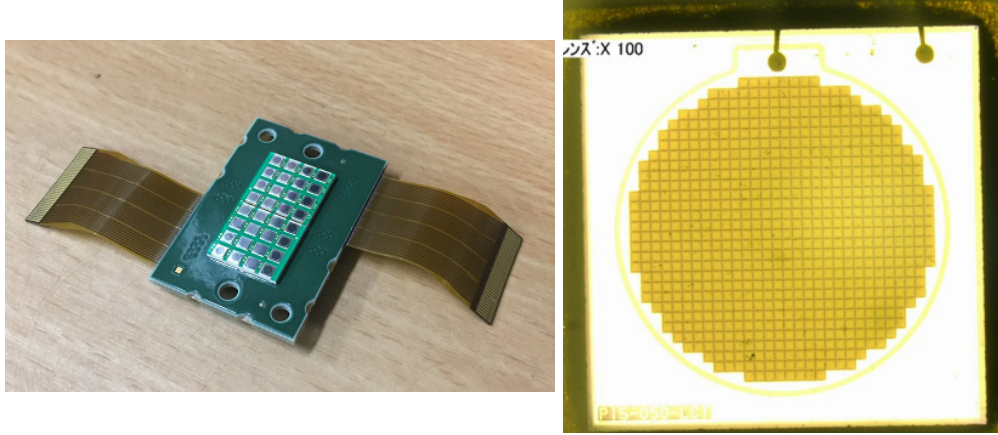


Figure 7: 32-channel arrayed MPPC (left) and an enlarged view of one MPPC channel (right).

2.2 INGRID Proton module

INGRID Proton module is a neutrino detectors of the T2K experiment. It is a fully-active tracking detector which consists of only scintillator strips. The purpose of this Proton Module is to separate the neutrino interaction types by detecting the protons and pions together with the muons from the neutrino interactions, and to measure the neutrino cross section for each interaction type. It consists of 36 tracking planes surrounded by veto planes (Figure 9), where each tracking plane is an array of two types of scintillator strips. The 16 strips in the inner region have dimensions of $2.5\text{cm} \times 1.3\text{cm} \times 120\text{cm}$, while the 16 strips in the outer region have dimensions of $5\text{cm} \times 1\text{cm} \times 120\text{cm}$, making a plane of $120 \times 120\text{cm}^2$ in the horizontal and vertical directions. The former is the scintillator produced for the K2K SciBar detector [3] and the latter was produced for INGRID. The tracking planes are placed perpendicular to the beam axis at 23mm intervals. Since the strips are aligned in one direction, each tracking plane is sensitive to either the horizontal or vertical position of the tracks. The tracking planes are therefore placed alternating in the horizontal and vertical directions so that three-dimensional tracks can be reconstructed. The tracking planes also serve as the neutrino interaction target. As with the Wagasci modules, scintillation light is read out by a WLS fiber and MPPC.

It was installed at the neutrino beam axis on the SS floor of the T2K near detector hall in 2010, and had been used for neutrino cross section measurements. In August 2017, it was moved to the B2 floor of the T2K near detector hall by J-PARC T59 after getting the approval from T2K to use them. J-PARC T59 is performing a neutrino beam measurement using the detector from October 2017, and the measurement will continue until May 2018 as we will discuss in Sec. 4.

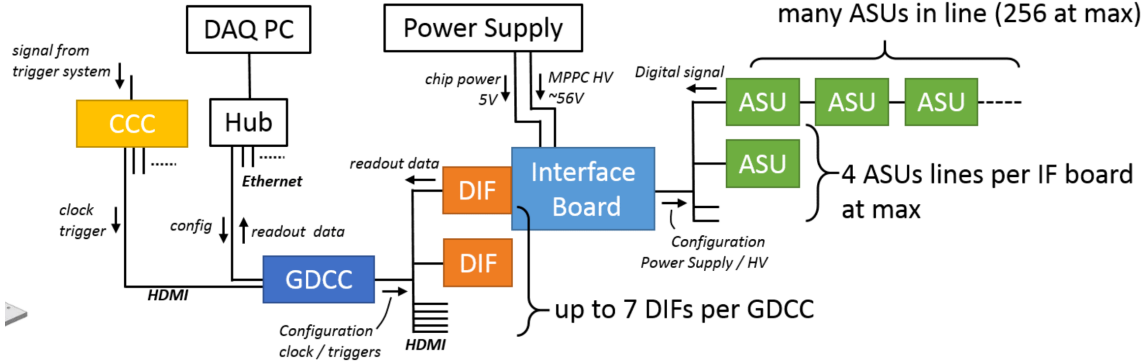


Figure 8: Wagasci electronics readout scheme.

216 We will operate the INGRID Proton module using the T2K near detector electronics/DAQ system in the same way as J-PARC T59. A proposal to use the module and its
 217 electronics for our project will be submitted to the T2K collaboration.
 218

219 **2.3 Baby MIND**

220 The Baby MIND is the downstream Muon Range Detector. It also works as a magnet and
 221 provides the charge identification capability as well as magnetic momentum measurement
 222 for high energy muons.

223 The Baby MIND collaboration ¹ submitted a proposal to the SPSC at CERN, SPSC-P-
 224 353. The project was approved by the CERN research board as Neutrino Platform project
 225 NP05 and constructed. The detector consists of 33 magnet modules, each 3500 mm ×
 226 2000 mm × 50 mm (30 mm steel) with a mass of approximately 2 tonnes. Of these magnet
 227 modules, 18 are instrumented with plastic scintillator modules.

228 **2.3.1 Magnet modules**

229 The Baby MIND is built from sheets of iron interleaved with scintillator detector modules
 230 but unlike traditional layouts for magnetized iron neutrino detectors (e.g. MINOS) which
 231 tend to be monolithic blocks with a unique pitch between consecutive steel segments and
 232 large conductor coils threaded around the whole magnet volume, the Baby MIND iron
 233 segments are all individually magnetized as shown in Fig. 10, allowing for far greater
 234 flexibility in the setting of the pitch between segments, and in the allowable geometries
 235 that these detectors can take.

236 The key design outcome is a highly optimized magnetic field map. A double-slit con-
 237 figuration for coil winding was adopted to increase the area over which the magnetic flux

¹Contact person: E. Noah, Spokesperson: A. Blondel, Deputy spokesperson: Y. Kudenko

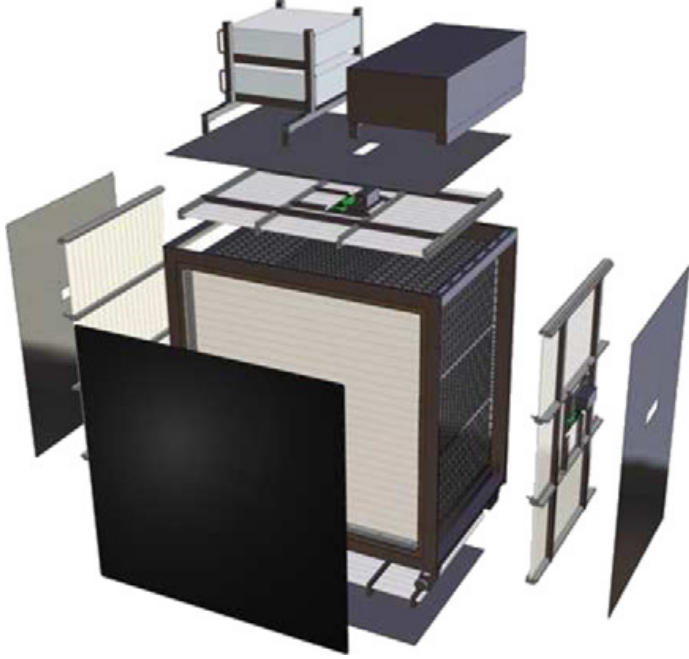


Figure 9: Schematic view of INGRID Proton module.

lines are homogeneous in B_x across the central tracking region. Simulations show the magnet field map to be very uniform over this central tracking region covering an area of $2800 \times 2000 \text{ mm}^2$, Fig. 11. The B_x component dominates in this region, with negligible B_y and B_z . This was confirmed by measuring the field with 9 pick-up coils wound around the first module. Subsequent modules were equipped with one pick-up coil. Test results on the 33 modules show all to achieve the required field of 1.5 T for a current of 140 A, with a total power consumption of 11.5 kW. The polarity of the field map shown in Fig. 11 (middle) can be reversed by changing the power supply configuration.

2.3.2 Scintillator modules

Each of the 18 scintillator modules is constructed from 2 planes of horizontal counters (95 counters in total) and 2 planes of vertical counters (16 counters in total) [2], arranged with an overlap between planes to achieve close to 100% hit efficiency for minimum ionizing muons. The arrangement of planes within a module is vertical-horizontal-horizontal-vertical. This arrangement was the result of an assembly approach whereby each plane was built from 2 half-planes, with each half plane consisting of a horizontal plane and a vertical plane. The scintillator bars are held in place using structural ladders that align and maintain the counters, Fig. 12. No glue is used in the process, so counters can be

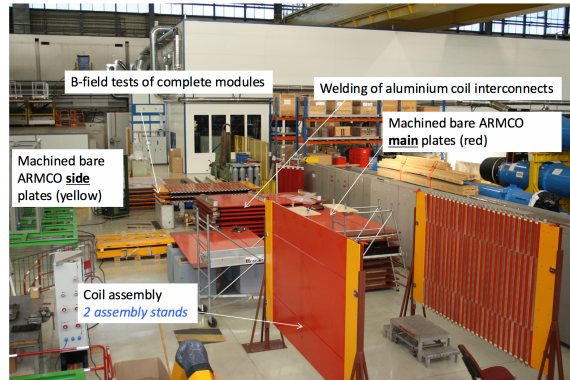


Figure 10: Magnet assembly zone at CERN.

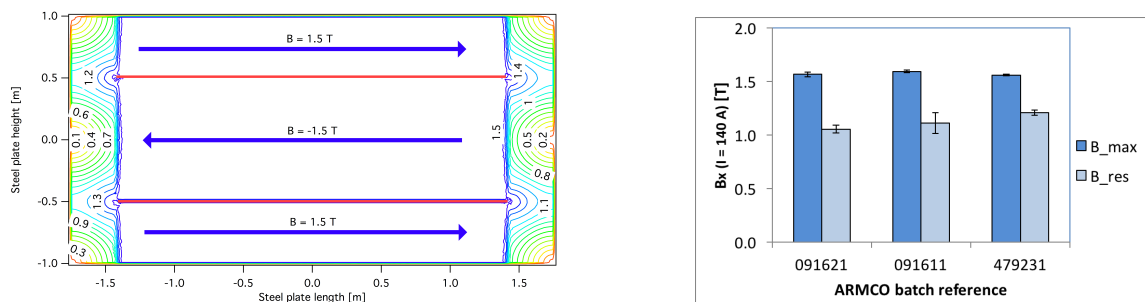


Figure 11: Left) Magnetic field map with a coil along 280 cm of the length of the plate. Right) Measured B field for 33 modules.

255 replaced. Aluminum sheets front and back provide light tightness.



Figure 12: Scintillator modules assembly. Left) top of front half-module showing vertical counters, and the spacers-ladders that set the pitch between horizontal counters and hold them in place. Middle) rear half-module showing horizontal counters on their ladders. Right) Assembled rear half-module, the front half-module can be seen in the background.

256 The plastic scintillator counters were made from 220 mm-wide slabs, consisting of
257 extruded polystyrene doped with 1.5% paraterphenyl (PTP) and 0.01% POPOP. They were
258 cut to size then covered with a 30-100 μm thick diffuse reflector resulting from etching of
259 the surface with a chemical agent [9, 10]. The horizontal counter size is $2880 \times 31 \times 7.5 \text{ mm}^3$,
260 with one groove along the length of the bar in which sits a wavelength shifting fiber from
261 Kuraray. The vertical counter size is $1950 \times 210 \times 7.5 \text{ mm}^3$, with one U-shaped groove
262 along the bar. On each counter, two custom connectors house silicon photomultipliers,
263 MPPC type S12571-025C from Hamamatsu, either side of the horizontal counter, and
264 both connectors at the top for the vertical counter. This geometrical configuration for
265 vertical counters was chosen for ease of connectivity to the electronics, and maintenance
266 operations.

267 A total of 1744 horizontal counters and 315 vertical counters (including spares) were
268 produced at the Uniplast company (Vladimir, Russia).

269 **2.3.3 Electronics**

270 The Baby MIND electronic readout scheme includes several custom-designed boards [11].
271 The revised version is shown in Fig. 13. At the heart of the system is the electronics
272 Front End Board (FEB), developed by the University of Geneva. The readout system
273 includes two ancillary boards, the Backplane, and the Master Clock Board (MCB) whose
274 development has been managed by INRNE (Bulgarian Academy of Sciences) collaborators.

275 The FEBv2 hosts 3 CITIROC chips that can each read in signals from 32 SiPMs [6].
276 Each signal input is processed by a high gain, and a separate low gain, signal path. The
277 outputs from the slow shapers can be sampled using one of two modes: a mode with an
278 externally applied delay, and a peak detector mode. A faster shaper can be switched to
279 either HG or LG paths, followed by discriminators with adjustable thresholds providing 32
280 individual trigger outputs and one OR32 trigger output. An Altera ARIA5 FPGA on the

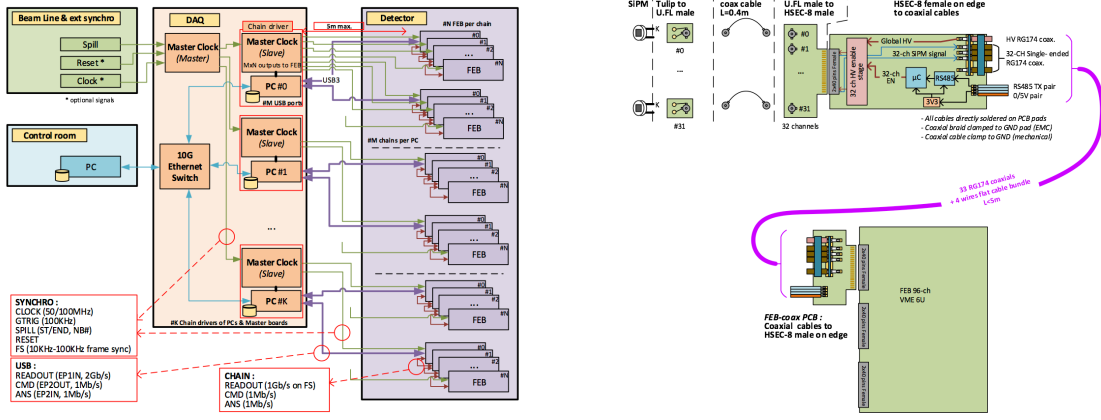


Figure 13: Left) Baby MIND electronics readout scheme. Right) SiPM-to-FEB connectivity.

281 FEBv2 samples these trigger outputs at 400 MHz, recording rising and falling times for
 282 the individual triggers and assigning time stamps to these. Time-over-threshold from the
 283 difference between falling and rising times gives some measure of signal amplitude, used in
 284 addition to charge information and useful if there is more than one hit per bar within the
 285 deadtime due to the readout of the multiplexed charge output of $\sim 9 \mu\text{s}$. The ARIA5 also
 286 manages the digitization of the sampled CITIROC multiplexed HG and LG outputs via a
 287 12-bit 8-ch ADC.

288 The internal 400 MHz clock on the FEBv2 can be synchronized to a common 100 MHz
 289 clock. The synchronization subsystem combines input signals from the beam line into
 290 a digital synchronization signal (SYNC) and produces a common detector clock (CLK)
 291 which can eventually be synchronised to an external experiment clock. Both SYNC and
 292 CLK signals are distributed to the FEBs. Tests show the FEB-to-FEB CLK(SYNC) delay
 293 difference to be 50 ps (70 ps). Signals from the beam line at WAGASCI include two
 294 separate timing signals, arriving 100 ms and 30 μs before the neutrino beam at the near
 295 detectors. The spill number is available as a 16-bit signal.

296 2.3.4 Pefromance check

297 All counters were measured at INR Moscow with a cosmic ray setup using the same type
 298 S12571-025C MPPCs and CAEN DT5742 digitizer. The average light yield (sum from both
 299 ends) was measured to be 37.5 photo-electrons (p.e.) per minimum ionizing particle (MIP)
 300 and 65 p.e./MIP for vertical and horizontal counters, respectively. After shipment to
 301 CERN, all counters were tested once more individually with an LED test setup [?]. 0.1% of
 302 counters failed the LED tests and were therefore not used during the assembly of modules.
 303 The assembly of modules was completed in June 2017, and it was then tested in June and

304 July 2017 at the Proton Synchrotron experimental hall at CERN with a mixed particle
 305 beam comprising mostly muons whose momenta could be selected between 0.5 and 5 GeV/c.
 An event display from the summer 2017 tests is shown in Fig. 14.

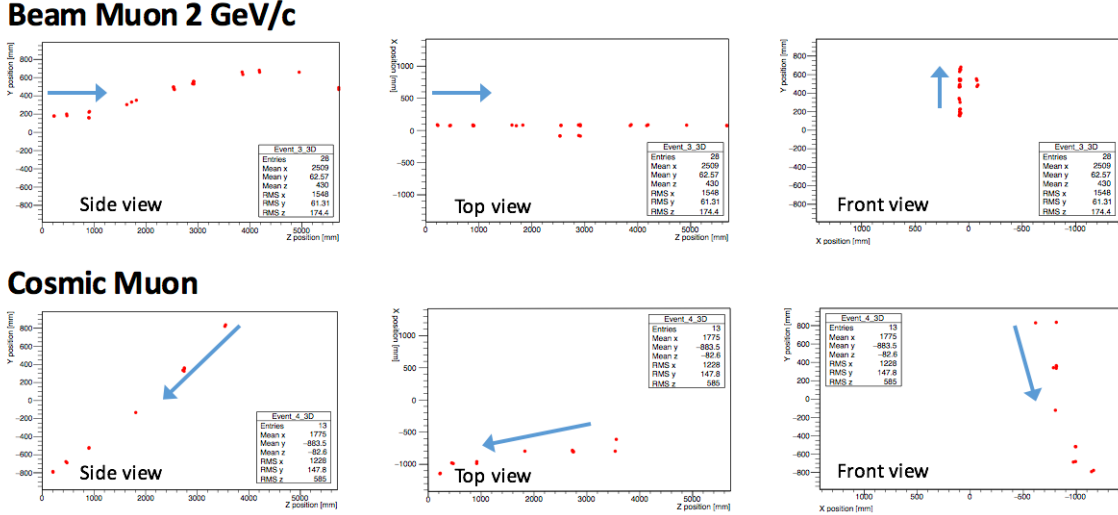


Figure 14: Comparison of a beam muon and cosmic muon in the three different geometrical projections of the detector. The beam impinges on the detector from the left. The arrows indicate the direction of travel of these muons. The direction of the cosmic muon is inferred from timing information.

306

307 2.4 Side muon range detector

308 Two Side-MRD modules for tracking secondary particles from neutrino interactions will be
 309 installed in 2018. Each Side-MRD module is composed of 11 steel plates and 10 layers of
 310 total 80 scintillator slabs installed in 13 mm gaps between the 30 mm thick plates. Each
 311 steel plate size is $30 \times 1610 \times 1800$ mm 3 . Total module size is $2236 \times 1630 \times 975$ mm 3 as
 312 shown in Fig. 15 (left), weight is ~ 8.5 ton.

313 Scintillator bars were manufactured by Uniplast company in Vladimir, Russia. Polystyrene
 314 based scintillators were extruded with thickness of 7 mm, then cut to the size of $7 \times 200 \times$
 315 1800 mm 3 . Dopant composition is 1.5% PTP and 0.01% POPOP. Scintillator surface was
 316 etched by a chemical agent to form a white diffuse layer with excellent reflective perfor-
 317 mance. Ideal contact between the scintillator and the reflector raises the light yield up to
 318 50% comparing to an uncovered scintillator. Sine like groove was milled along the scin-
 319 tillator to provide uniform light collection over the whole scintillator surface. WLS Y11
 320 Kuraray fiber of 1 mm diameter is glued with an optical cement EJ-500 in the S-shape
 321 groove as shown in Fig. 15(right). Bending radius is fixed to 30 mm that was specified to

322 be safe for Kuraray S-type fibers. Both ends of the fiber are glued into optical connectors
 323 which mounted within a scintillator body and provide an interface to SiPMs, Hamamatsu
 324 MPPC S13081-050CS(X1).

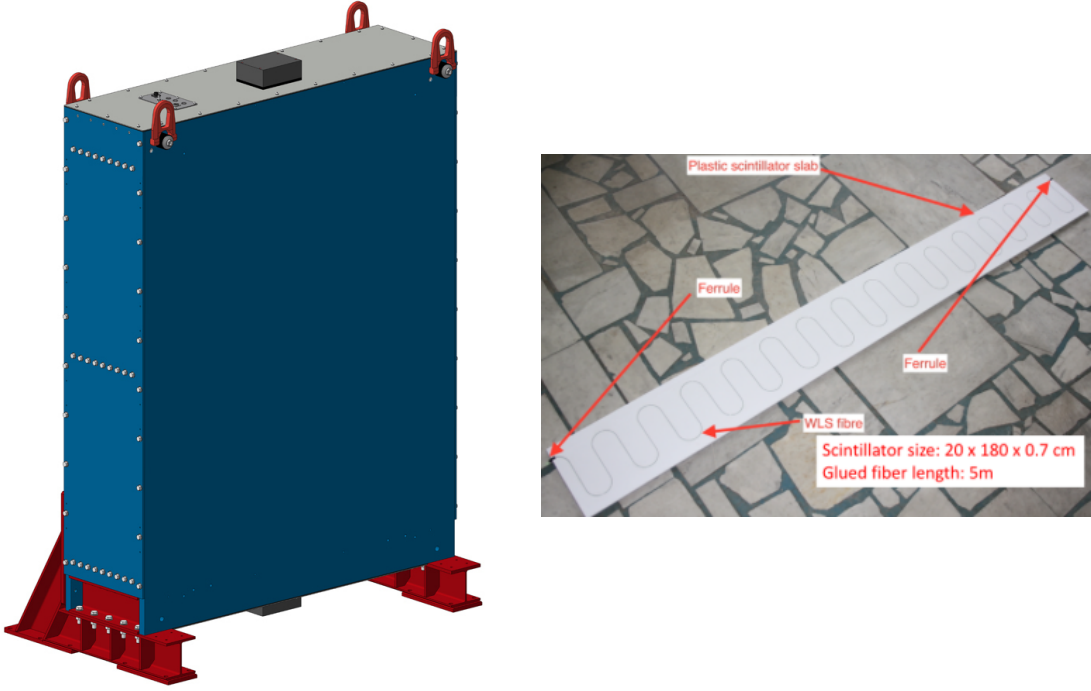


Figure 15: Left :Side-MRD module. Right: Scintillator bar of the Side-MRD modules.

325 Scintillators for the Side-MRD modules had been assembled at INR in Russia, and
 326 shipped to Japan in July 2017. The light yield for each scintillator was measured with
 327 cosmic rays at INR and at YNU in Japan after delivery. Parameters measured at the
 328 center of the counter were : the light yields LY_1 and LY_2 at both ends, the light yield
 329 asymmetry between the ends calculated as $100\% \times \frac{LY_1 - LY_2}{LY_1 + LY_2}$. After tests at INR we selected
 330 324 counters from measured 332 ones with the mean light yield of 45 p.e./MIP ($LY_1 + LY_2$
 331) and the asymmetry value less than 10 %. The measurements at YNU yielded the average
 332 total light yield of about 40 p.e./MIP which varies in range from 32 to 50 p.e./MIP (Fig.
 333 16 (left)). Only two counters showed relatively high asymmetry close to 25 % as shown in
 334 Fig. 16 (right). Using the results of the quality assurance test we selected 320 scintillator
 335 counters for the Side-MRD modules.

336 We also measured the time resolution for a combination of four counters piled each on
 337 another one. The average result for four counters is $\sigma_T = 1.04$ ns. The resolution of com-

338 bination of 2, 3, 4 counters is measured to be 0.79 ns, 0.66 ns and 0.58 ns, correspondently.

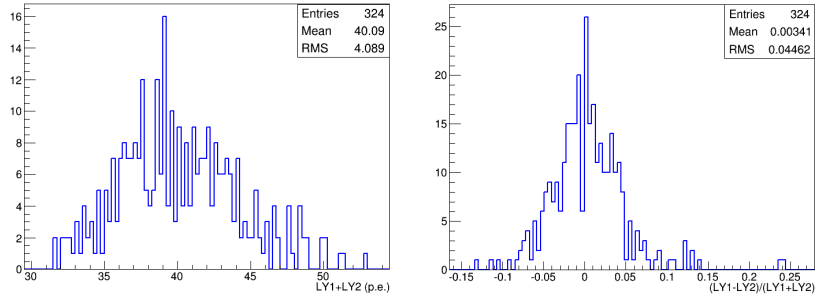


Figure 16: Total light yield distribution (left) and light yield assymetry (right) measured at YNU.

339
340 Construction of Side-MRD modules will be done from November 2017 at Yokohama
341 National University, then they will be transported to J-PARC and will be installed at B2
342 floor of the T2K near detector hall.

343 Same electronics as the WAGASCI modules (see Sec. 2.1.2) are used for the Side-MRD
344 modules.

345 3 Physics goals

346 We will measure the differential cross section for the charged current interaction on H₂O
347 and Hydrocarbon(CH)). The water-scintillator mass ratio of the Wagasci module is as
348 high as 5:1 and the high purity measurement of the cross section on H₂O is possible. One
349 experimental option is to remove water from one of the two Wagasci modules. The water-
350 out WAGASCI module will allow to measure pure-CH target interactions with very low
351 momentum-threshold for protons. It will also benefit to subtract the background from
352 interaction with scintillator in the water target measurement. Another option is to add
353 the T2K proton module which is fully made of plastic scintillators. It will allow the high
354 statistics comparison of cross section between H₂O and CH and also comparison with
355 the ND280 measurement. The actual configuration will be optimized with detailed MC
356 simulation by 2018 Summer.

357 Our setup allows the measurements of inclusive and also exclusive channels such as 1- μ ,
358 1- $\mu 1p$, 1- $\mu 1\pi \pm np$ samples, former two of which are mainly caused by the quasi-elastic and
359 2p2h interaction and the latter is mainly caused by resonant or coherent pion production
360 and deep elastic scattering. In general, an accelerator produced neutrino beam spectrum
361 is wide and the energy reconstruction somehow rely on the neutrino interaction model.

362 Therefore, recent neutrino cross section measurement results including those from T2K
363 are given as a flux-integrated cross section rather than cross sections as a function of
364 the neutrino energy to avoid the model dependency. We can provide the flux-averaged
365 cross section. In addition, by combining our measurements with those at ND280, model-
366 independent extraction of the cross section for narrow energy region becomes possible.
367 This method was demonstrated in [1] and also proposed by P** (NUPRISM).

368 3.1 Expected number of events

369 Expected number of neutrino events after the event selections is evaluated with Monte
370 Carlo simulations as we will discuss in Section 5. In the neutrino-mode, 4.2×10^3 , 1.1×10^3
371 and 3.8×10^3 CC neutrino events are expected in the water-in WAGASCI module, the
372 water-out WAGASCI module and the INGRID proton module after the selections with
373 0.5×10^{21} POT, and its purities are 78.0 %, 97.5 % and $\sim 98\%$. In the antineutrino-mode,
374 1.7×10^3 , 0.4×10^3 and 1.5×10^3 CC antineutrino events are expected in the water-in
375 WAGASCI module, the water-out WAGASCI module and the INGRID proton module
376 after the selections with 0.5×10^{21} POT, and its purities are 59.5 %, 74.4 % and $\sim 74\%$.

377 Statical errors of flux integrated CC-inclusive neutrino cross section measurements on
378 H₂O (full acceptance) and CH targets (forward acceptance) will be 1.5 % and 1.6 % with
379 0.5×10^{21} POT in the neutrino-mode. Statical errors of flux integrated CC-inclusive an-
380 tineutrino cross section measurements on H₂O (full acceptance) and CH targets (forward
381 acceptance) will be 2.4 % and 2.5 % with 0.5×10^{21} POT in the antineutrino-mode.

382 Statical errors of flux integrated H₂O to CH CC-inclusive neutrino cross section ratio
383 measurement will be 3.1 % (full acceptance) and 2.3 % (forward acceptance) with 0.5×10^{21}
384 POT in the neutrino-mode. Statical errors of flux integrated H₂O to CH CC-inclusive
385 antineutrino cross section ratio measurement will be 5 % (full acceptance) and 3.7 %
386 (forward acceptance) with 0.5×10^{21} POT in the antineutrino-mode.

387 3.2 Pseudo-monochromatic beam by using different off-axis fluxes

388 The off-axis method gives narrower neutrino spectrum, and the peak energy is lower for
389 larger off-axis angle. There still remains high energy tail mainly due to neutrinos from
390 Kaon decay. The off-axis angle of the Wagasci location is 1.5 degree and different from the
391 ND280 2.5 degree. Top two plots of Fig. 17 show the energy spectra of fluxes and neutrino
392 interaction events at these two different location. The high energy tail of ND280 flux can
393 be somehow subtraction by using the Wagasci measurement. The low energy part of the
394 Wagasci flux can be also subtracted by using the ND280 measurement. Bottom two plots
395 of Fig. 17 demonstrate this method. We can effectively get two fluxes, from 0.2 GeV to
396 0.9 GeV and 0.6 GeV and 2 GeV and measure flux-integrated cross section for these two
397 fluxes.

398 Statical errors of flux integrated CC-inclusive neutrino cross section measurements

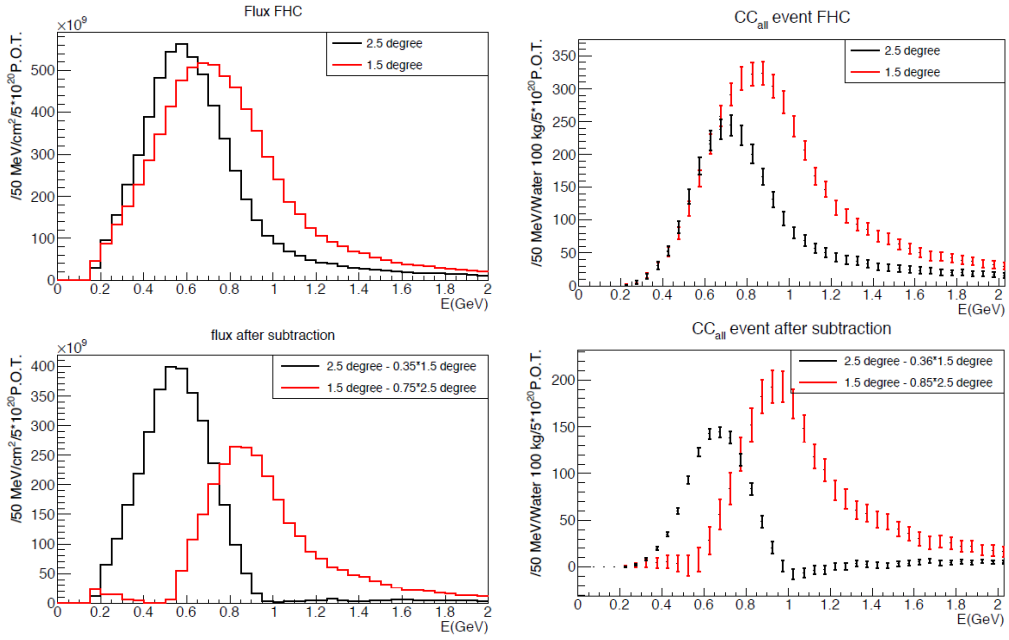


Figure 17: Energy spectra obtained by using different off-axis angle fluxes. Top two plots show the fluxes(left) and spectra of interaction events (right) for ND280 (off-axis 2.5 degree) and Wagasci (off-axis 1.5 degree). Bottom two plots show the fluxes (left) and spectra of interaction events (right) obtained by subtraction of fluxes at ND280 and Wagasci. The error bar is for the statistical error and those in the bottom right plot is obtained assuming the statistical error for ND280 measurement is much smaller than that of Wagasci experiment.

399 on H₂O (forward acceptance) and CH targets (forward acceptance) with the pseudo-
400 monochromatic beam will be 2 % and 1.9 % with 0.5×10^{21} POT in the neutrino-mode.
401 Statical errors of flux integrated CC-inclusive antineutrino cross section measurements
402 on H₂O (forward acceptance) and CH targets (forward acceptance) with the pseudo-
403 monochromatic beam will be 3 % and 2.8 % with 0.5×10^{21} POT in the neutrino-mode.

404 3.3 Subjects Wagasci can contribute

405 In T2K experiment, neutrinos interact with bound nucleons in relatively heavy nuclei
406 (Carbon and Oxygen), so the cross-section is largely affected by nuclear effects. The nuclear
407 effects are categorized as nucleons' momentum distribution in nucleus, interactions with
408 correlated pairs of nucleons in nucleus (two particles-two holes, 2p2h), collective nuclear
409 effects and final state interactions (FSI) of secondary particles in the nuclei after the initial

410 neutrino interactions.

411 The 2p2h interactions mainly happen through Δ resonance interactions following a
 412 pion-less decay and interactions with a correlated nucleon pair. The 2p2h interactions are
 413 observed in electron scattering experiments [7] where the 2p2h events observed in the gap
 414 between Quasi-Elastic region and Pion-production region as shown in Fig. 18. Neutrino
 415 experiments also attempt to measure the 2p2h interactions, but separation of the QE peak
 416 and the 2p2h peak is more difficult because transferred momentum (p) and energy (w)
 417 are largely affected by neutrino energies which cannot be determined event-by-event in the
 418 wide energy spectrum of the accelerator neutrino beam. Our model-independent narrow
 419 neutrino spectra extracted from combined analyses of our data and ND280 data are ideal
 420 for searching the 2p2h interaction because clearer separation of the QE peak and the 2p2h
 421 peak is expected. Another way to observe the 2p2h interaction is direct measurement of
 422 proton tracks in CC0 π sample with low detection threshold and full acceptance. Fig. 19
 423 shows proton multiplicities after FSI in CCQE events and 2p2h events, and Fig. 20 shows
 424 opening angles among two proton tracks in the same samples. The water-out Wagasci
 425 can provide good sample for the 2p2h interaction search because its low density medium
 426 enables the detection of low momentum protons in addition to the full acceptance.

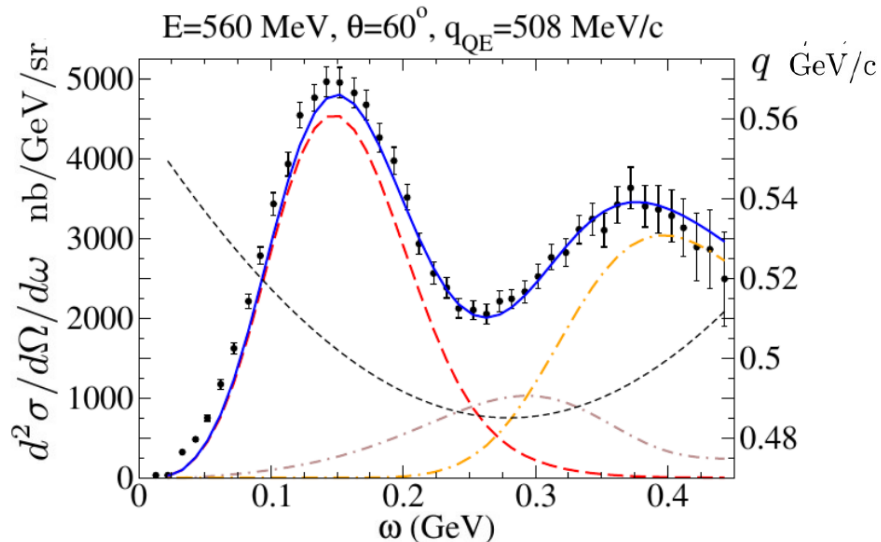


Figure 18: Comparison of inclusive $^{12}\text{C}(\text{e},\text{e}')$ cross sections and predictions of the QE-SuSAv2 model (long-dashed red line), 2p-2h MEC model (dot-dashed brown line) and inelastic-SuSAv2 model (long dot-dashed orange line) (from Ref. [7]). The sum of the three contributions is represented with a solid blue line. The q dependence with w is also shown (short-dashed black line.)

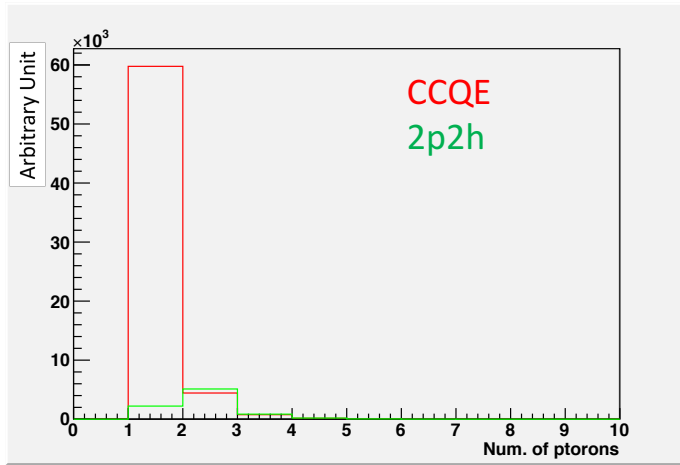


Figure 19: Proton multiplicities after FSI in CCQE events and 2p2h events.

427 There are various models which describe the collective nuclear effects [8]. The Q^2
 428 dependence of the effects can be tested by measuring angular distribution of muons in
 429 CC1- μ and CC1- $\mu 1p$ events. The uncertainties of the effects in low (high) Q^2 regions can
 430 be constrained by observing the events with a forward-going (high-angle) muon, so it is
 431 essential to measure muon tracks with full acceptance.

432 T2K experiment is starting to use ν_e CC1 π events for its CP violation search to increase
 433 the statistics. One of the biggest uncertainty of the CC1 π sample comes from the final
 434 state interactions of pions in the nuclei after the initial neutrino interactions because they
 435 change the multiplicity, charge and kinematics of the pions. The multi-pion production
 436 events can be migrated into the CC1 π sample due to the FSIs, and they become important
 437 backgrounds. We can constrain the uncertainties from the pion FSIs by measuring pion
 438 rescattering in the detector and pion multiplicity in ν_μ CCn π sample with low detection
 439 threshold and full acceptance for pion tracks. The water-out WAGASCI can provide good
 440 sample for the pion FSI studies because its low density medium enables the detection of
 441 low momentum pions in addition to the full acceptance.

4 Status of J-PARC T59 experiment

443 We had submitted a proposal of a test experiment to J-PARC in April 2014 to test a new
 444 detector with a water target, WAGASCI, at the neutrino monitor hall, and the proposal
 445 was approved as J-PARC T59. The project contains the side and downstream muon range
 446 detectors as well.

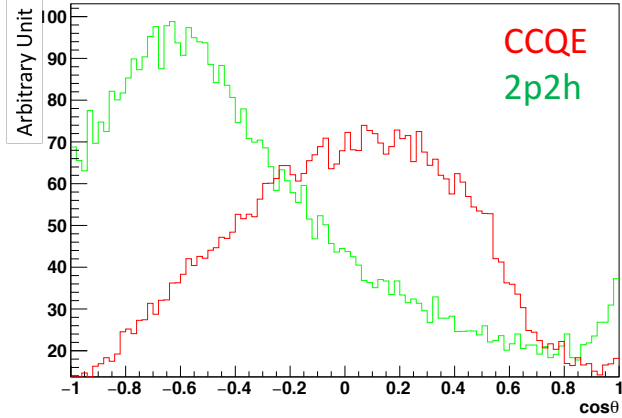


Figure 20: Opening angles among two proton tracks after FSI in CCQE events and 2p2h events.

447 The first WAGASCI module has been constructed in 2016 and installed at the on-
 448 axis position in front of the T2K INGRID detector for the commissioning and the first
 449 cross section measurement as a part of the T2K experiment. The INGRID electronics
 450 boards are used to read the signal. The light yield measured with muons produced by
 451 the interaction of neutrinos in the hall wall, shown in Fig. 21, is sufficiently high to get
 452 good hit efficiency. A track search algorithm based on the cellular automaton has been
 453 developed using the software tools by the T2K INGRID. Examples of observed events are
 454 shown in Fig. 22. The tracking efficiency in 2-dimensional projected plane was evaluated
 455 by comparing the reconstructed track in the WAGASCI module and the INGRID module
 456 and shown in Fig. 23. Note that that the tracking efficiency for high angle (> 70 deg) is not
 457 evaluated because of the acceptance of the INGRID module, not because of the limitation
 458 of the WAGASCI module.

459 In 2017 Autumn, the construction of the second WAGASCI module and the dedicated
 460 electronics board were completed. The module and the electronics were install to the B2
 461 floor together with the T2K proton module and the INGRID module as shown in Fig. 24.
 462 The proton module is to be used as the entering muon veto and also for the comparison
 463 of interaction between CH and Water. The INGRID module is for the temporary muon
 464 detector with limited acceptance for this period. The detector was commissioned and is
 465 in operation to take data with the antineutrino beam during the T2K beam time from
 466 October.

467 The production of the components of the side muon range detectors has been completed

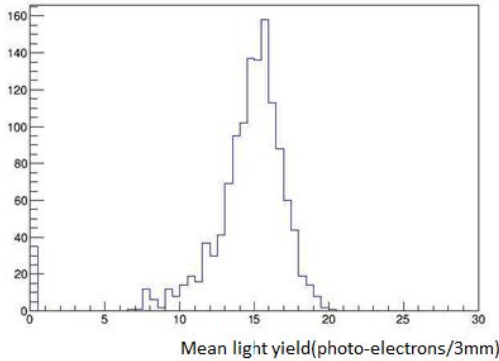


Figure 21: Light yield for muons produced by the interaction of neutrinos in the hall wall. Average light yields for each channel are plotted.

468 and now the detectors are being assembled at the Yokohama National University. These
 469 detectors will be installed sometime from January to June, 2018 when T2K is not running.
 470

The Baby MIND detector was transported from CERN to Japan in December, 2017.
 471 It will be installed and commissioned in Jan.-Feb. 2018 and T59 will take the neutrino-
 472 induced muon data in April and May.

473 5 MC studies

474 5.1 Simulation setup

475 Simulation study was conducted by using the T2K neutrino flux generator, JNUBEAM,
 476 neutrino interaction simulator, NEUT, and Geant4 for the detector responses.

477 The detector geometry in the simulation so far is different from the actual setup as
 478 shown in Fig. 25. The active neutrino target region consists of four WAGASCI modules.
 479 The size of the WAGASCI module is same as the actual one: 100 cm \times 100 cm in the
 480 x and y directions and 50 cm along the beam direction (z-direction). Two Side-MRD
 481 modules is installed at both sides of the WAGASCI modules, and each Side-MRD module
 482 consists of ten iron plates whose dimension is 3 cm (thickness) \times 200 cm (height) \times 320 cm
 483 (width). The distance between the Side-MRD modules and WAGASCI modules is 80 cm.
 484 The downstream-MRD is equivalent to the Baby-MIND, but without the magnetic field.
 485 It consists of thirty iron plates whose dimension is 3 cm (thickness) \times 200 cm (height)
 486 \times 400 cm (width). The distance between the downstream-MRD modules and WAGASCI
 487 modules is 80 cm. Update of the study with the actual geometry is now underway.

488 To simulate the signal, the energy deposit inside the scintillator is converted into the

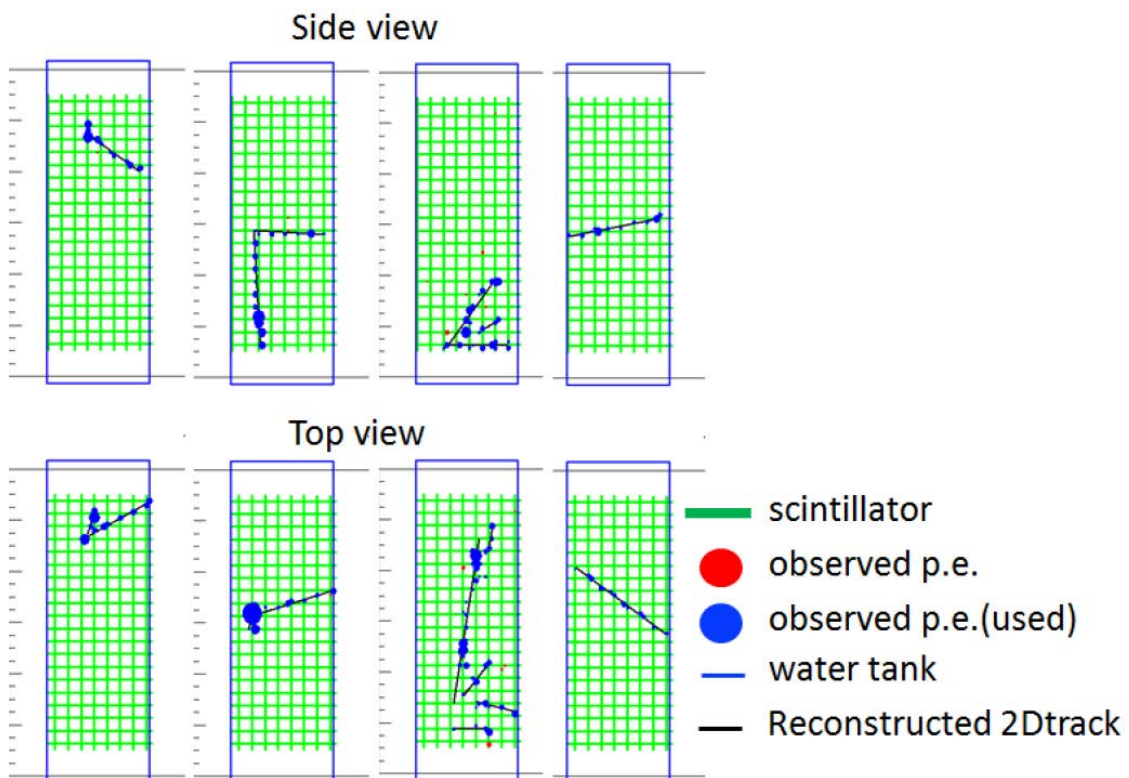


Figure 22: Example event displays of the WAGASCI module at on-axis. The reconstructed tracks are overlaid.

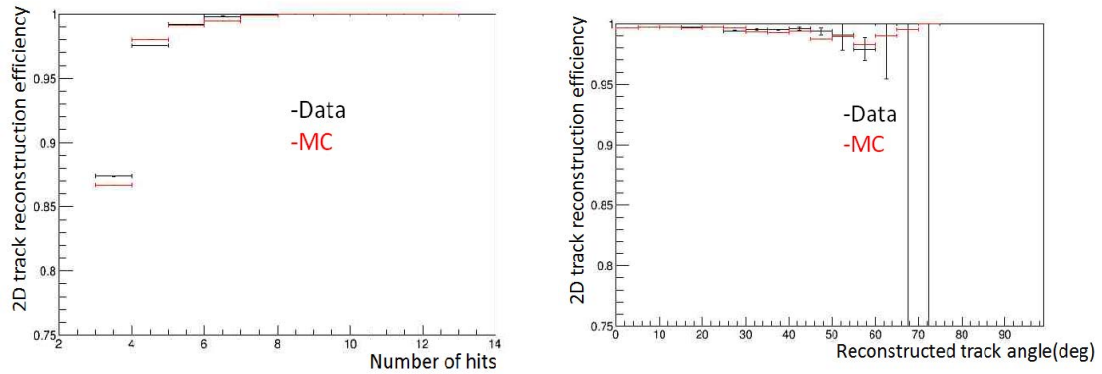


Figure 23: 2D track reconstruction efficiency as a function of number of hits (left) and track angle (right). Here the track angle is the one reconstructed by the INGRID module.

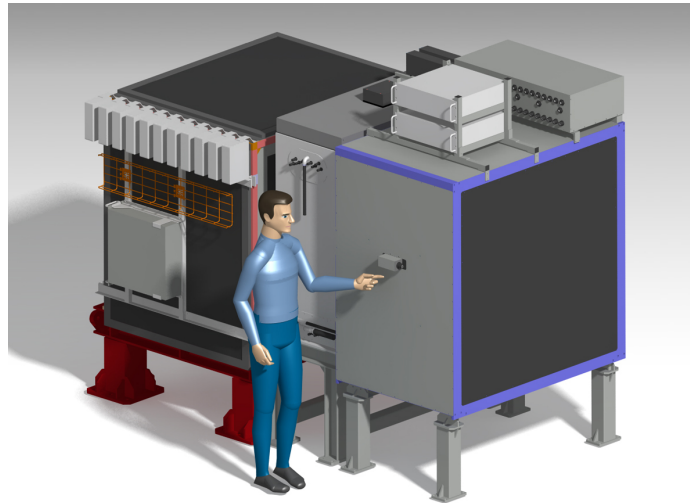


Figure 24: J-PARC T59 detector configuration in October 2017.

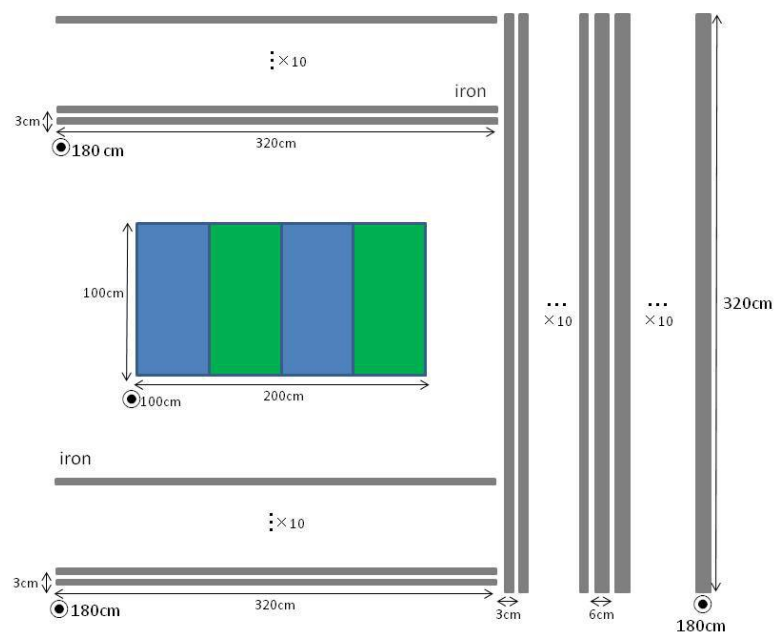


Figure 25: Geometry of the detectors in the Monte Carlo simulation.

489 number of photons. The effects of collection and attenuation of the light in the scintillator
490 and the WLS fiber are simulated, and the MPPC response is also taken into account. The
491 light yield is smeared according to statistical fluctuations and electrical noise.

492 **5.2 Event selection**

493 Tracks are reconstructed in two-dimensional planes in each sub-detector. Then, track
494 matching among the sub-detectors and three-dimensional track reconstruction are per-
495 formed. These analysis tools have been developed from the software tools by the T2K
496 INGRID and in mature stage already.

497 The events are selected as follows. The starting point of the track is required to be
498 5 cm away from the edge of the WAGASCI module. This is to remove the background
499 from the outside. The longest track has to penetrate more than one (five) iron plates in
500 Side-MRD modules (Baby-MIND). This cut select a muon track and rejects backgrounds
501 from NC and neutral particles. Then, in order to determine the muon momentum, it is
502 required that the longest track stops in MRDs (Side-MRD modules and Baby-MIND) or
503 penetrate all iron plates.

504 Table 1 shows numbers of the selected events in one water-in WAGASCI module after
505 the event selection. We expect 4,239 (1,666) events from charged-current interaction on
506 water with 5×10^{20} POT in (anti)neutrino-mode with one water-in WAGASCI module.
507 The purity, when interactions on CH is counted as background, is 78% for the neutrino-
508 mode. There is a significant contamination from the wrong-sign (neutrino) interaction for
509 antineutrino-mode, however, we expect that it will be removed with efficiency higher than
90% by Baby MIND.

Table 1: Expected number of the selected neutrino-candidate events in one water-in WA-
GASCI module with 5×10^{20} POT in each of neutrino-mode and antineutrino-mode. Note
that the wrong sign component will be reduced by one order by applying the charge selec-
tion by Baby MIND.

	CC on water	NC on water	Interaction on CH	wrong sign interaction
ν -mode	4239	107	1087	(negligible)
anti- ν -mode	1666	14	560	(561)

510
511 Table 2 and ?? summarize contributions classified by the interaction types and final
512 state topologies for the selected charged current-interaction events, respectively.

513 Figure 26 shows the reconstructed angles of the longest tracks in the selected events in
514 the neutrino-mode and the anti-neutrino mode. Figure ?? shows the iron plane numbers
515 in Side-MRD and Baby-MIND corresponding to the end points of the longest tracks in the
516 selected events in the neutrino-mode and the anti-neutrino mode.

Table 2: Interaction types for the selected charged-current events.

	CCQE	2p2h	CC resonant π	CC-DIS
ν -mode	48.4 %	9.7 %	27.1 %	14.7 %
anti- ν -mode	57.1 %	8.2 %	17.3 %	17.3 %

Table 3: Final state topologies for the selected charged-current events.

	CC0 π	CC1 π	CC2 π	CCn π
ν -mode	67.4 %	20.9 %	3.0 %	8.7 %
anti- ν -mode	79.5 %	16.3 %	1.2 %	3.0 %

517 6 Standalone WAGASCI-module performances

518 In the previous sections, the WAGASCI detector was studied using the Muon Range Detectors. In this section, the standalone abilities of WAGASCI module are presented. Using
 519 the WAGASCI configuration presented in Section 5, we have evaluated that only 7% of
 520 the muons will be stopped in one of the WAGASCI modules. THower, this proportion
 521 increases to 53% for pions and 73% for protons produced by neutrino interactions at 1.5°
 522 off-axis. Figure 28 shows the momentum distribution of these daughter particles as well as
 523 for the sub-sample stopped in one of the WAGASCI modules. Therefore, the study of the
 524 standalone abilities of the WAGASCI module in this section are dominantly motivated by:
 525

- 526 • the accurate measurement of the neutrino interaction final states. Though most of the
 527 muons will be reconstructed and identified in the MRDs, the hadronic particles will
 528 predominantly stops in one WAGASCI module. One has therefore to rely exclusively

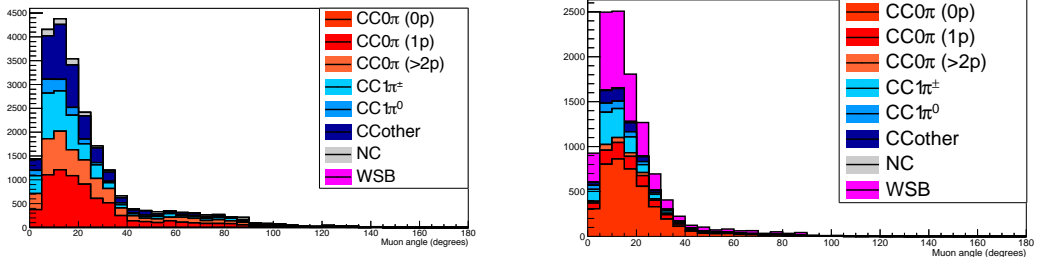


Figure 26: The reconstructed angles of the longest tracks in the selected events in the neutrino-mode (left) and the antineutrino-mode (right).

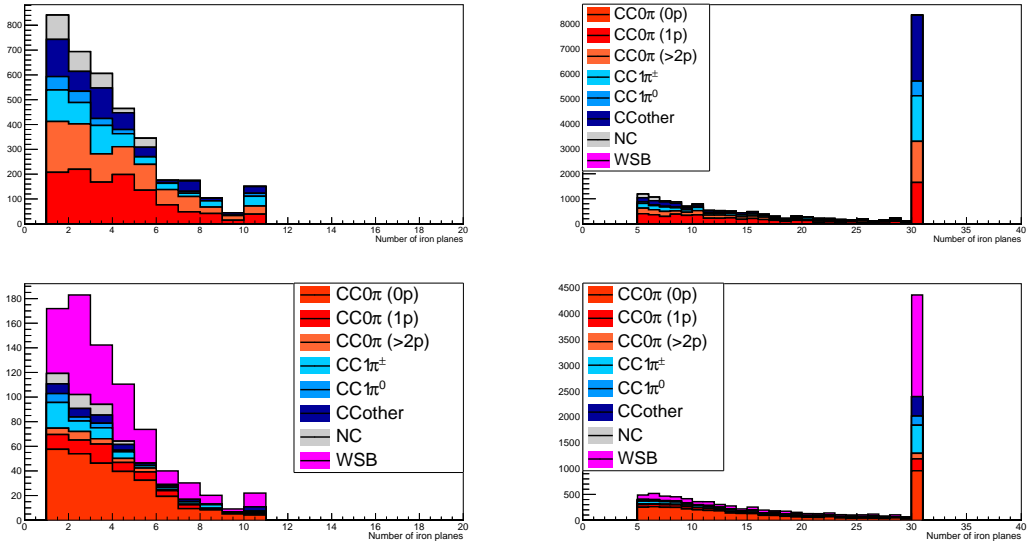


Figure 27: Iron plane numbers in Side-MRD (left) and Baby-MIND (right) corresponding to the end points of the longest tracks in the selected events in the neutrino-mode (top) and the antineutrino-mode (bottom).

529 on the WAGASCI module information alone to reconstruct, identify and measure the
 530 momentum of pions or protons.

- 531 • the coverage of the MRDs is not 4π . Using the WAGASCI module information can
 532 therefore help to constraint the particles that exits the WAGASCI module but do
 533 not geometrically enters any MRD.
- 534 • the particle identification of low momenta $p_\mu < 300$ MeV/c that will leave only
 535 few hits in the MRD. Using the WAGASCI module information will clearly enhance
 536 the particle identification.

537 This study is based on an original study done for the ND280 upgrade target, with some
 538 modifications. Though the cell size is similar to the WAGASCI configuration presented
 539 in Section 5, the external dimensions are different ($186.4 \times 60 \times 130$ cm 3). Whenever the
 540 results are presented with this external size and this parameter is likely to impact the
 541 result, it will be mentioned.

542 Note that in this section, a simplified reconstruction algorithm presented in Section 6.1 is
 543 used. The fiducial volume is chosen accordingly as the inner cube of the module which
 544 surfaces are distant of $4 \times$ scintillator space = 10 cm from the module external surfaces.
 545 The neutrino interactions are simulated using NEUT v5.3.2. The NEUT input neutrino

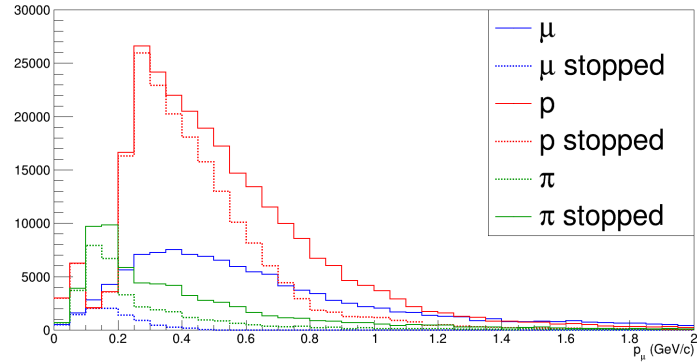


Figure 28: Momentum distribution of true particles in WAGASCI (plain) and corresponding distributions only for particles stopping into the WAGASCI module (dashed).

flux is estimated using JnuBeam v13a and assuming the detector to be located at 1.5° off-axis, as in Section 5. Note that the event reconstruction efficiency as a function of true neutrino energy might be changed at 1.5° , due for example to different Q^2 distributions. For this reason, one has to note that the reconstruction results might slightly be changed from 2.5° and 1.5° . To avoid a similar change on the particle-only reconstruction efficiencies, they will be presented as a function of variables that completely characterize the particle kinematic state, *i.e.* its momentum and angle. Figure 29 shows the vertices distributions of the daughter particles of neutrinos interacting one standard WAGASCI water-module. In this section, we will show the detector reconstruction and particle identification in this phase space, both for leptonic and hadronic particles. We will finally show an empty WAGASCI module can highly enhance the ability to constrain the neutrino interaction final state which is critical to reduce the corresponding uncertainties.

558 6.1 Reconstruction algorithm

559 6.1.1 Description

560 For this section, an ideal “simulated” reconstruction is developed. A particle is recon-
561 structed if:

- 562 1. The particle is charged.
- 563 2. Lets at least one hit (energy deposit > 2.5 photo-electron) in a scintillator.
- 564
- 565 3. The particle enters one TPC and let one hit in the tracker.
566 Or
567

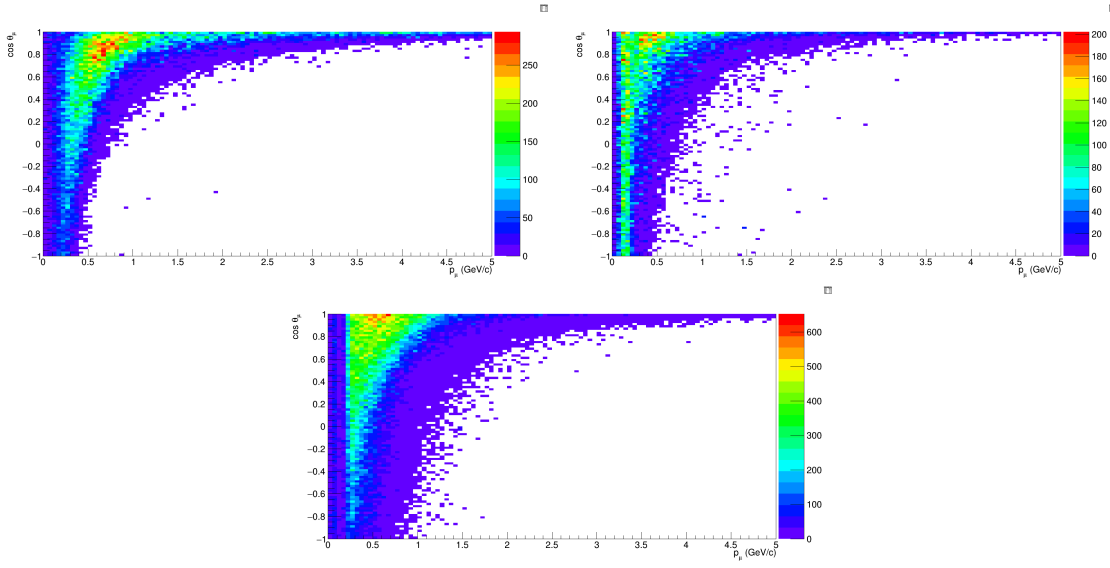


Figure 29: True number of muons (left), charged pions (right) and protons (bottom) in the two WAGASCI water-module as a function of the particles momenta and angles at 1.5° .

- The particle should be long enough to be reconstructed by the detector in at least 2 out of 3 views (XZ, YZ, XY). The length criterion requires the particle to let at least 4 hits in the detector. In the “less favourable case” of pure longitudinal or transverse going tracks, it represents a the track length of $L_{track} \geq 4 \times$ scintillator space = 10.0 cm.
- In the views where particles pass the length criterion, the particle shall not be superimposed with longer tracks in at least two views. The superposition criterion is estimated with the distance inter-tracks (DIT) which corresponds to the orthogonal distance between two tracks at the ending point of the shortest one (see Figure 30). For a track 1, the superposition criterion is tested with every longer tracks that starts at the same vertex. Let \vec{p}_1^a the vector of track 1, and p_1^a its projections in the XZ, YZ and XY planes respectively for $i=1,2,3$. Note that these are projections in a 2D planes and not on a direction vector. In this case, the relative angle between the track 1 and a longer track 2 (of vector \vec{p}_2^a) in a view a is given by:

$$\cos \theta = \frac{\vec{p}_1^a \cdot \vec{p}_2^a}{\|\vec{p}_1^a\| \|\vec{p}_2^a\|} \quad (1)$$

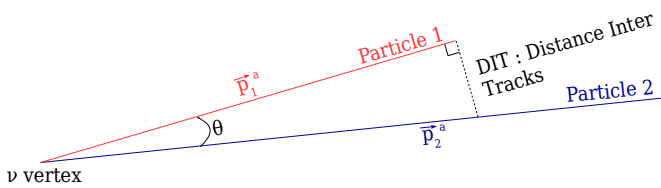


Figure 30: Definition of the distance inter tracks.

583 and the distance inter track is given by:

$$584 \quad DIT = \|\vec{p}_1^a\| \sin \theta \quad (2)$$

585 The DIT should be higher than $4 \times$ scintillator width for the track 1 to be not
 586 superimposed with the track 2 in the view a, which also corresponds to 10.0 cm
 in the nominal configuration.

587 **6.1.2 Performances**

588 The particle-only reconstruction efficiencies and the reconstruction threshold in momenta
 589 are shown in Table 4. This threshold is defined as the maximal momentum for which the
 590 reconstruction efficiency is smaller than 30%. The thresholds in muon and pion momenta
 591 are 150 MeV/c. Most of the muons are above this threshold (see Figure 29) which leads
 592 to a 79% reconstruction efficiency.

	μ	π	p
Reconstruction Efficiency	79%	52%	26%
Momentum threshold	150 MeV/c	150 MeV/c	550 MeV/c

Table 4: Reconstruction efficiency and momentum threshold for muons, pions and protons. The threshold is defined as the maximal momentum for which particles have a reconstruction efficiency smaller than 30%.

593 The lower pion and proton efficiencies (respectively 52% and 26%) are due to lower
 594 efficiencies for similar momenta than muons, coming from strong interactions as shown
 595 on Figures 31. Efficiencies of each particle type tend to decrease in the backward region
 596 due to particle lower momenta. However, for a fixed momentum value, the reconstruc-
 597 tion efficiency is almost uniform which confirms the ability of the WAGASCI detector to
 598 reconstruct high angle tracks.

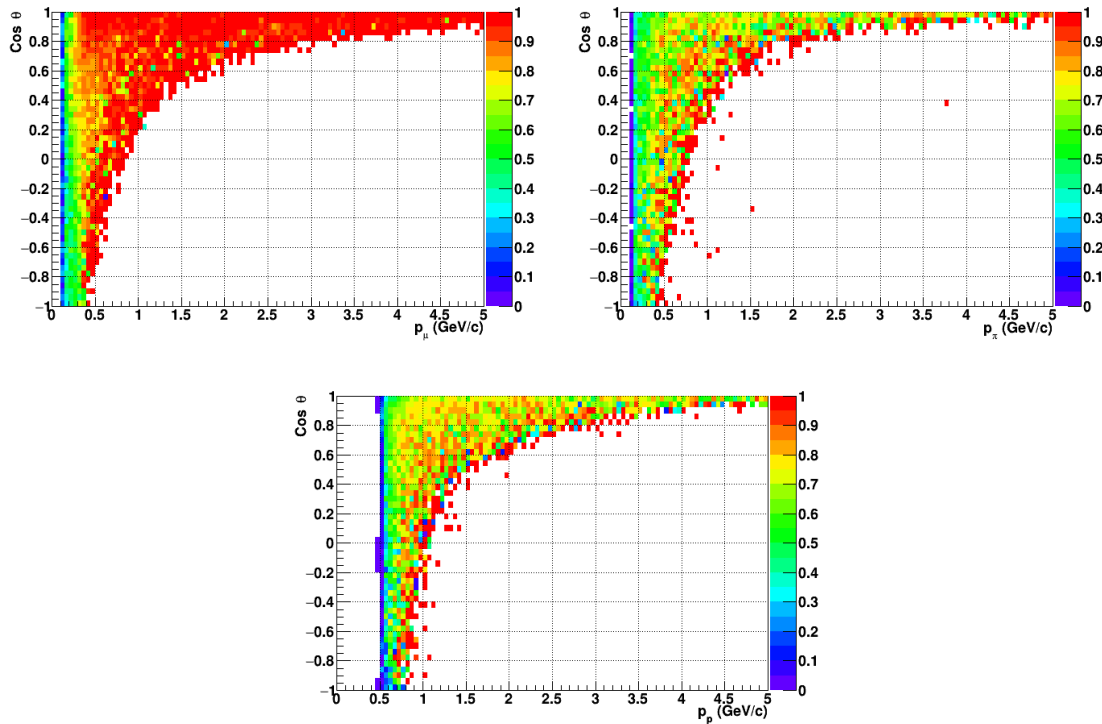


Figure 31: Reconstruction efficiency of muons (left), charged pions (right) and protons (bottom) in the WAGASCI water-module as a function of the particles momenta and angles.

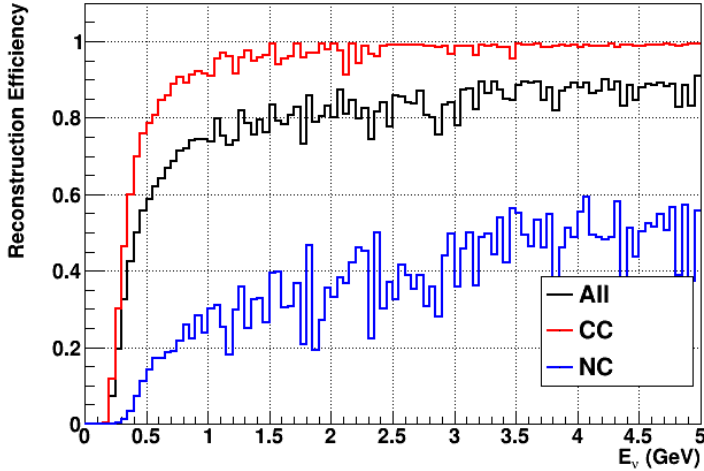


Figure 32: Reconstruction efficiency of all neutrino (black), CC (red) and NC (blue) interactions in the WAGASCI water-module as a function of the neutrino energy.

599 The reconstruction is thereafter tested on neutrino events. Table 5 summarizes the
 600 number of reconstructed events and efficiencies for each interaction type. As expected
 601 from the high muon reconstruction efficiency, the charged current interactions have recon-
 struction efficiencies $\geq 85\%$.

	CC0 π	CC1 π	CCOthers	NC	All
Reconstruction efficiency	85%	87%	91%	22%	68%

Table 5: Number of true interactions reconstructed. The purity and reconstruction effi-
 ciency of each true interaction is also shown.

602
 603 The reconstruction efficiencies as a function of the neutrino energy and muon kinematics
 604 are respectively shown on Figure 32 and 33.

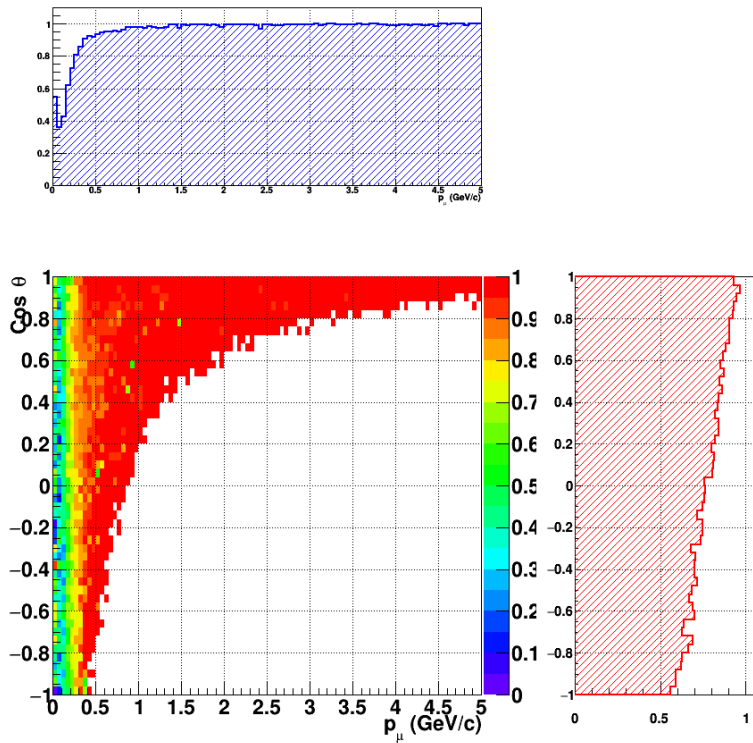


Figure 33: Reconstruction efficiency of CC interactions in the WAGASCI water-module as a function of the muon kinematic variables (momentum and angle).

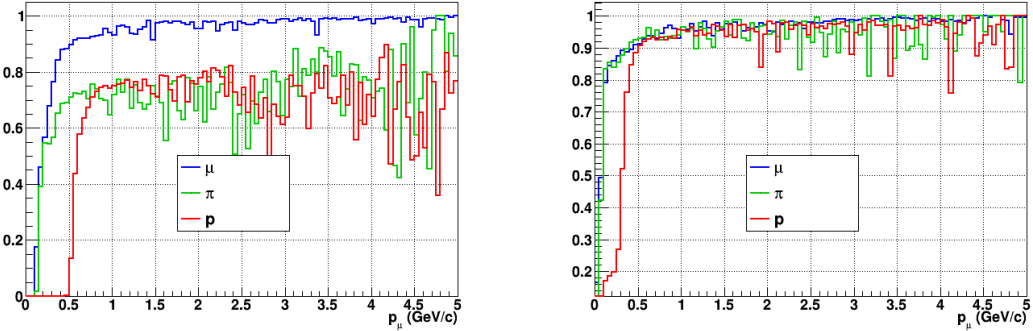


Figure 34: Reconstruction efficiency for muons, pions and protons in the water-in (left) and water-out (right) modules.

Note that a Particle Identification Algorithm has been also developed. It is based on the charge deposition of the particles in the scintillator, of the detection of a decay-electron. However, this information highly depends on the number of scintillator hit by a particle, which creates an important difference between a real WAGASCI module and the one used for the ND280-upgrade simulation. For this reason, the corresponding results will not be detailed here, but can be found in [?].

6.2 Background subtraction: the water-out module

In the nominal configuration, 20% of the neutrino interactions occurs on scintillators (C_8H_8). This background should be removed in order to measure the neutrino interaction on the same target as Super-K, which suppress the differences in cross-section models. For this purpose, we propose to use a water-out module, where the water is replaced by air. The detector is therefore fully active and has a 3 mm spatial resolution (scintillator thickness) which create an ideal detector to reconstruct and identify hadrons, and study np-nh interactions. The counter-part is the difference in particle energy deposition between the water and this water-out module that will need to be corrected for. In this section, we present the capabilities of such a module, and the impact it can have on cross-section measurements for the neutrino community in general and T2K in particular. The same reconstruction and selection as the water-in module is applied. Figure 34 shows the comparison between the water-in and the water-out reconstruction efficiencies for muon, pions and protons. 90% of the muons and 87% of the pions are reconstructed, while 70% of the protons are even reconstructed. It allows to lower down the proton threshold to 250 MeV/c (see Table 6).

As a consequence of tracking even low momenta particle, the reconstruction efficiency is uniform and almost maximal on the entire $\cos \theta_\mu$ phase space, as shown on Figure 35.

	μ	π	p
Reconstruction Efficiency Momentum threshold	90% 50 MeV/c	87% 50 MeV/c	70% 250 MeV/c

Table 6: Reconstruction efficiency, proportions of μ -like and non μ -like and momentum threshold for muons, pions and protons in the empty module. The threshold is defined as the maximal momentum for which particles have a reconstruction efficiency smaller than 20%.

629 Since the fiducial mass represents 0.25 tons, the total number of events is divided by a
 630 factor of 3 compared to the water-in module. The water-out module offers interesting
 631 possibilities to study np-nh interaction since 70% of the protons are reconstructed. In the
 632 future, a possible separation as a function of the number of proton track will be studied.
 633 Moreover, we are currently pursuing the use of single and double transverse variables (cite
 634 Xianguo) to open new possibilities for separating np-nh from Final State Interactions, or
 635 for isolating the interactions on hydrogen from interactions on carbon in this module.

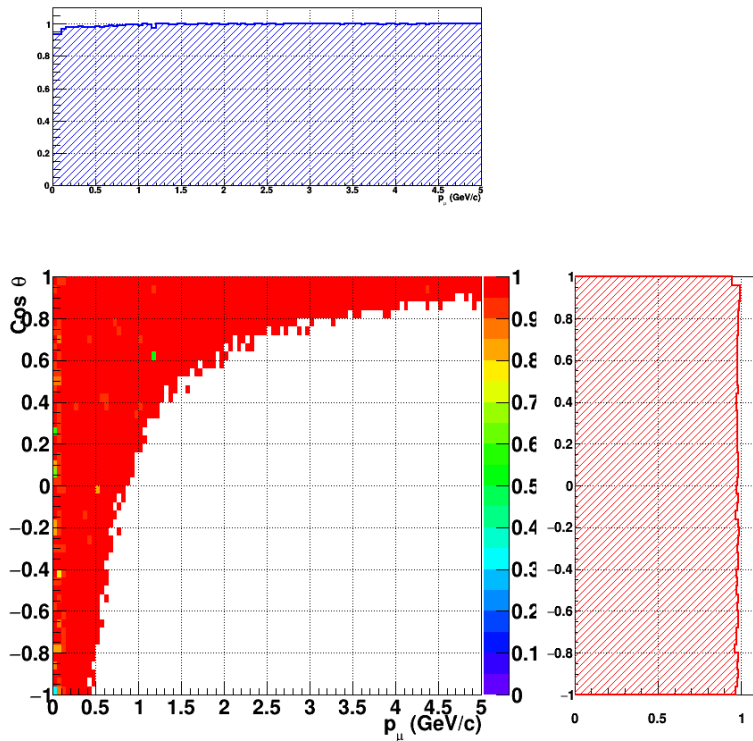


Figure 35: Reconstruction efficiency of CC interactions in the WAGASCI empty module as a function of the muon kinematic variables (momentum and angle).

636 **7 Schedule**

637 We would like to start a physics data taking from T2K beam time after the summer
638 shutdown in 2018. By then, commissioning and tests of the detectors will be completed
639 in J-PARC T59. The experiment can run parasitically with T2K, therefore we request no
640 dedicated beam time nor beam condition as discussed in the following section.

641 Once the approved POT is accumulated, the WAGASCI modules will be removed
642 from the experimental site, but we would like to keep the Baby-MIND and the Side-MRD
643 modules on the B2 floor of the NM pit as common platforms of future neutrino experiments
644 using the T2K neutrino beam.

645 **8 Requests**

646 **8.1 Neutrino beam**

647 The experiment can run parasitically with T2K, therefore we request no dedicated beam
648 time nor beam condition. As data taking periods, we request the ‘nominal’ T2K one-year
649 operation both for the neutrino beam and the antineutrino beam. The T2K has been
650 requesting 0.9×10^{21} POT/year and actually accumulating about 0.7×10^{21} POT/year in
651 recent years. For each year, starting from the Autumn, T2K is running predominantly in
652 the neutrino mode or in the antineutrino mode. Our request is to have one-year neutrino-
653 mode data and another one-year antineutrino mode data assuming that the POT for the
654 fast extraction in each year is more than 0.5×10^{21} POT.

655 **8.2 Equipment request including power line**

656 We request the followings in terms of equipment on the B2 floor:

- 657 • Site for the WAGASCI modules, Side-MRD modules and BabyMIND and their elec-
658 tronics system on the B2 floor of the near detector hall (Fig. 2 and 3).
- 659 • Anchor points (holes) on the B2 floor to secure the WAGASCI modules, Side-MRD
660 module and Baby-MIND, detailed floor plans to be communicated in a separate
661 document.
- 662 • Power line for the magnets in Baby-MIND: 400 V tri-phase 48-to-62 Hz, capable of
663 delivering 12 kW. We have a wish for the magnet power line to be installed and
664 available to us by beginning of March 2018.
- 665 • Electricity for electronics and water circulation system, 3 kW, standard Japanese
666 electrical sockets.

- 667 1. Online PCs: 2.1 kW

668 2. Electronics: 0.7 kW

669 3. Water sensors: 1 kW

- 670 • Air conditioner for cooling heat generation at Baby-MIND magnets, online PCs and
671 electeronics
- 672 • Beam timing signal and spill information
- 673 • Network connection

674 The infrastructure for much of the above exists already. Exceptions are the power line
675 for the magnet and the electronics and holes in the B2 floor to anchor the detector support
676 structures.

677 References

- 678 [1] K. Abe et al. Measurement of the muon neutrino inclusive charged-current cross
679 section in the energy range of 13 GeV with the T2K INGRID detector. *Phys. Rev.*,
680 D93(7):072002, 2016.
- 681 [2] M. Antonova et al. Baby MIND Experiment Construction Status. In *Prospects in*
682 *Neutrino Physics (NuPhys2016) London, London, United Kingdom, December 12-14,*
683 2016, 2017.
- 684 [3] K. Nitta et al. The k2k scibar detector. *Nucl. Instrum. Meth. A*, 535:147, 2004.
- 685 [4] K. Abe et al. (T2K Collaboration). Measurement of the inclusive ν_μ charged current
686 cross section on iron and hydrocarbon in the t2k on-axis neutrino beam. *Phys. Rev.*
687 D, 90:052010, 2014.
- 688 [5] F. Magniette F. Gastaldi, R. Cornat and V. Boudry. A scalable gigabit data acquisition
689 system for calorimeters for linear collider. *proceedings of TIPP2014*, page PoS 193,
690 2014.
- 691 [6] J. Fleury, S. Callier, C. de La Taille, N. Seguin, D. Thienpont, F. Dulucq, S. Ahmad,
692 and G. Martin. Petiroc and Citiroc: front-end ASICs for SiPM read-out and ToF
693 applications. *JINST*, 9:C01049, 2014.
- 694 [7] M. B. Barbaro J. A. Caballero T. W. Donnelly G. D. Megias, J. E. Amaro. Inclusive
695 electron scattering within the susav2 meson-exchange current approach. *Phys. Rev.*
696 D, 94:013012, 2016.
- 697 [8] M. Valverde J. Nieves, J. E. Amaro. Inclusive quasi-elastic neutrino reactions. *Phys.*
698 *Rev. C*, 70:055503, 2004.

- 699 [9] Yu. G. Kudenko, L. S. Littenberg, V. A. Mayatsky, O. V. Mineev, and N. V. Ershov.
700 Extruded plastic counters with WLS fiber readout. *Nucl. Instrum. Meth.*, A469:340–
701 346, 2001.
- 702 [10] O. Mineev, Yu. Kudenko, Yu. Musienko, I. Polyansky, and N. Yershov. Scintillator
703 detectors with long WLS fibers and multi-pixel photodiodes. *JINST*, 6:P12004, 2011.
- 704 [11] Etam Noah et al. Readout scheme for the Baby-MIND detector. *PoS*, Photo-
705 toDet2015:031, 2016.
- 706 [12] Omega. Spiroc 2 user guide. 2009.